Check for updates

Geophysical Research Letters

RESEARCH LETTER
10.1029/2025GL115163

Aerosol Influences on Cloud Water: Insights From ARM EPCAPE Observations With Explainable Machine Learning

Haipeng Zhang[1,2,3], **Yunyan Zhang**[1], **Zhanqing Li**[2,3], **and Youtong Zheng**[4,5]

[1]Lawrence Livermore National Laboratory, Livermore, CA, USA, [2]Department of Atmospheric and Oceanic Science, University of Maryland, College Park, MD, USA, [3]Earth System Science Interdisciplinary Center, University of Maryland, College Park, MD, USA, [4]Department of Earth and Atmospheric Science, University of Houston, Houston, TX, USA, [5]Institute of Climate and Atmospheric Science, University of Houston, Houston, TX, USA

Abstract This study employs an explainable machine learning (ML) framework (XGBoost-SHapley Additive exPlanations analysis) to investigate controlling factors on cloud liquid water path (LWP) using EPCAPE observations near the California coast. Aerosols are found to be the dominant factor explaining LWP variability, surpassing meteorological factors (MFs). By isolating aerosol effects from meteorological influences, the ML reveals a negative linear relationship between LWP and cloud droplet number concentration (N_d) in log space, likely driven by entrainment drying via evaporation-entrainment feedback. This aligns with the negative regime of the inverted-V relationship reported in previous studies, while no positive LWP responses are found due to a limited number of precipitating cases in EPCAPE. Furthermore, the sensitivity of LWP to N_d shows a non-linear dependence on MFs like moisture contrast between surface and free troposphere and lower-tropospheric stability. This occurs due to the interplay between the MFs' direct effects on entrainment drying and indirect effects through LWP adjustments.

Plain Language Summary This study uses an explainable machine learning approach to understand further how environmental factors influence cloud water by isolating aerosols effect from the co-influence of meteorological factors (MFs). Using field campaign observations near the California coast, we find that aerosols play a more significant role in controlling cloud water than MFs such as moisture contrast between the surface and free troposphere (dq) and lower-tropospheric stability (LTS). Our analysis reveals that more aerosols tend to reduce cloud water, likely because they make clouds lose moisture by enhancing the entrainment of dry air from the free troposphere due to increased evaporation. We also explore how MFs (i.e., dq and LTS) influence the sensitivity of cloud water to aerosols, exhibiting a non-linear impact, as a result of the interplay between the MF's direct and indirect influence on entrainment drying. This study underscores the capability of explainable ML to disentangle complex aerosol-cloud interactions and offers valuable insights for constraining and refining warm-cloud microphysics parameterizations in future research.

Key Points:

- Explainable machine learning identifies aerosols as the top factor linked to cloud water variability, outweighing meteorology in ARM Eastern Pacific Cloud Aerosol Precipitation Experiment observations
- Liquid water path decreases with more aerosols, suggesting consistency with entrainment drying effects
- Meteorological factors, such as humidity contrast across the lower atmosphere, non-linearly modulate aerosol effects on cloud water

Supporting Information:

Supporting Information may be found in the online version of this article.

Correspondence to:

H. Zhang and Y. Zhang,
hpzhang@umd.edu;
zhang25@llnl.gov

Citation:

Zhang, H., Zhang, Y., Li, Z., & Zheng, Y. (2025). Aerosol influences on cloud water: Insights from ARM EPCAPE observations with explainable machine learning. *Geophysical Research Letters*, *52*, e2025GL115163. https://doi.org/10.1029/2025GL115163

Received 29 JAN 2025
Accepted 17 JUL 2025
Corrected 23 DEC 2025

This article was corrected on 23 DEC 2025. See the end of the full text for details.

© 2025 The Author(s).
This is an open access article under the terms of the Creative Commons Attribution-NonCommercial License, which permits use, distribution and reproduction in any medium, provided the original work is properly cited and is not used for commercial purposes.

1. Introduction

Marine stratocumulus clouds significantly cool Earth's climate due to their extensive coverage and high reflectivity, which allows them to reflect sunlight more effectively than other cloud types (Hahn & Warren, 2007; Warren et al., 1986, 1988). Meanwhile, their low height renders a weak warming effect due to thermal emissions. These clouds are susceptible to aerosol particles situated chiefly in the marine boundary layer (MBL) that serve as cloud condensation nuclei (CCN), impacting their micro- and macro-physical properties and hence their cloud radiative forcing. In terms of microphysical properties, an increase in CCN leads to higher cloud droplet number concentration (N_d) and smaller cloud droplets for a given liquid water path (LWP), enhancing cloud albedo and brightening the clouds, the Twomey effect (Twomey, 1977). Changes in CCN can also alter the cloud macrophysical properties (i.e., cloud fraction and LWP), known as cloud adjustments, by affecting precipitation, cloud top entrainment, and boundary-layer stability, among other processes (e.g., Ackerman et al., 2004; Albrecht, 1989; Bretherton et al., 2007; Chun et al., 2023; Qiu et al., 2024; H. Wang et al., 2011). However, the radiative forcing from cloud adjustments, including both its sign and magnitude, remains highly uncertain (Bellouin et al., 2020), likely resulting from the intricate interactions between those physical processes.

Recently, increasing attention has been paid to the LWP adjustment to N_d, which is characterized by an inverted-V relationship: LWP first increases with rising N_d and then decreases, as evidenced in both satellite observations

19448007, 2025, 15, Downloaded from https://agupubs.onlinelibrary.wiley.com/doi/10.1029/2025GL115163 by University Of Houston, Wiley Online Library on [01/04/2026]. See the Terms and Conditions (https://onlinelibrary.wiley.com/terms-and-conditions) on Wiley Online Library for rules of use; OA articles are governed by the applicable Creative Commons License

(Arola et al., 2022; Goren et al., 2025; Gryspeerdt et al., 2019) and modeling studies (Hoffmann et al., 2020, 2024; Mülmenstädt, Ackerman, et al., 2024; Mülmenstädt, Gryspeerdt, et al., 2024). But the underlying causes of this inverted-V relationship remain controversial. Some argue for a causal relationship. Specifically, this LWP versus N_d pattern reflects two distinct sensitivity regimes: a positive regime for a precipitating MBL and a negative regime for a non-precipitating MBL. In the precipitating MBL, an increase in N_d leads to smaller cloud droplets, reducing the efficiency of collision coalescence, thereby suppressing precipitation and increasing LWP (Albrecht, 1989). On the other hand, in the non-precipitating MBL, higher N_d enhances the entrainment of dry air from the free troposphere into the clouds, through the sedimentation-entrainment effect (Ackerman et al., 2004; Bretherton et al., 2007) or the evaporation-entrainment feedback (S. Wang et al., 2003; Xue & Feingold, 2006), which results in decreased LWP.

However, such a causal explanation is confounded by other factors. In satellite observations, the observed negative sensitivity of LWP to N_d can result from the retrieval error in cloud effective radius, especially in non-raining clouds (Arola et al., 2022). The negative relationship may also arise from aerosol-LWP covariability driven by meteorological factors (MFs). A popular hypothesis is the airmass-history argument (George & Wood, 2010; Goren et al., 2025; Mülmenstädt, Gryspeerdt, et al., 2024): airmasses originating from continental regions typically carry higher aerosol concentrations but lower moisture compared to those from oceanic origins, leading to a negative correlation between N_d and LWP. This covariability is modulated by synoptic-scale meteorology that governs airmass advection and boundary-layer depth. For example, George and Wood (2010) found that over the Southeast Pacific, the negative N_d-LWP relationship in time is linked to the strengthening of the subtropical high near the coast. This intensification suppresses the MBL depth and LWP, while promoting offshore aerosol transport. Also, the covariability is evident in space (Goren et al., 2025; Mülmenstädt, Ackerman, et al., 2024): farther offshore, MBLs tend to be deeper due to weaker subsidence, which favors larger LWP, but lower in aerosol concentrations due to increased distance from continental sources. Therefore, to enhance our understanding of aerosol effects on LWP, further efforts are necessary, such as improving retrieval accuracy and isolating meteorology-induced co-variability.

The emergence of new ground observations of marine clouds and novel explainable machine learning (ML) approaches opens up new avenues for understanding cloud water responses to aerosols. The Eastern Pacific Cloud Aerosol Precipitation Experiment (EPCAPE, Russell et al., 2021), was recently conducted near San Diego, California, which is downwind from major pollution sources at the ports of Los Angeles and Long Beach. The site's exposure to a wide range of aerosol particle concentrations and the persistent presence of stratocumulus cloud layers makes it an ideal location for investigating cloud water responses to aerosols. Also, we employ the measurements of CCN made at a spectrum of supersaturations in the lower MBL (Uin & Enekwizu, 2024) to approximate N_d in certain conditions and these ground-based observations help sidestep the satellite retrieval errors that introduce spurious negative N_d-LWP relationships. To isolate the cofounding influence of meteorology, aerosol effects are usually examined through the data stratified by environmental factors (Fons et al., 2023; Liu et al., 2024). However, such studies usually consider only one or two MFs, potentially overlooking the influence of other meteorological variables or their interactions. Recently, an explainable ML approach, namely SHapley Additive exPlanations (SHAP, Lundberg & Lee, 2017; Lundberg et al., 2018), has proven effective in dissecting the physical controls in marine clouds by isolating the impact of each factor (Jia et al., 2024; Silva et al., 2022; H. Zhang et al., 2024a). This method is effective to distinguish the effects of aerosols on cloud water from those of key MFs. This study aims to leverage these EPCAPE observations and the SHAP analysis to thoroughly examine the N_d-LWP relationship, including its dependency on large-scale meteorology and its diurnal variations.

2. Data and Methodology

2.1. EPCAPE Observations

The EPCAPE was mainly conducted at a coastal site, the Scripps Pier in La Jolla, with a supplementary site at the Scripps Mt. Soledad nearby from February 2023 to February 2024 (Russell et al., 2021). It provides comprehensive observations of stratocumulus clouds in the Eastern Pacific, including their extent, radiative properties, and interactions with aerosols. The main-site observations are used for understanding the N_d-LWP relationship. The cloud properties and meteorological variables we adopt are given below.

19448007, 2025, 15, Downloaded from https://agupubs.onlinelibrary.wiley.com/doi/10.1029/2025GL115163 by University Of Houston, Wiley Online Library on [01/04/2026]. See the Terms and Conditions (https://onlinelibrary.wiley.com/terms-and-conditions) on Wiley Online Library for rules of use; OA articles are governed by the applicable Creative Commons License

The observed LWP is retrieved from the two-channel microwave radiometer (Turner et al., 2007). The number concentration of activated CCN is measured by CCN Counter (Dual Column) under a supersaturation ramping mode from 0.1% to 1.0% (Uin & Enekwizu, 2024), with ramping-averaged values used for analysis. This measurement approximates N_d, assuming the MBL is well-mixed throughout the measurement and much of measured CCN is activated in clouds. Based on the cloud-surface coupling criteria proposed by Z. Wang et al. (2016), we have examined the coupling states of our cases using radiosonde data and found that 76% are coupled, supporting our well-mixed assumption (Figure S1 in Supporting Information S1). Major chemical components of the aerosols observed in EPCAPE are total organics and sulfates (Figure S2 in Supporting Information S1). The profiles of temperature and moisture are taken from balloon radiosondes at the Scripps Pier site, 4 times per day at 02:00, 08:00, 14:00, and 20:00 Local Standard Time (Holdridge & Holdridge, 2020). Wind speeds and wind directions are obtained from the Surface Meteorological System (MET) (Kyrouac & Tuftedal, 2024). Surface sensible and latent heat flux (LHF) are from the Eddy CORrelation (ECOR) flux measurement system (Cook & Sullivan, 2020). The mixed-layer height is obtained from Planetary Boundary Layer Height (PBLH) Value Added Products retrieved from radiosondes using the Heffter method (Heffter, 1980). In our study, all variables are averaged hourly.

2.2. ERA5 Reanalysis Data

The 4-times-per-day observations of balloon radiosondes significantly limit the sample size in our analysis. To increase samples, we use hourly vertical meteorological data from the fifth-generation ECMWF reanalysis data (ERA5, Hersbach et al., 2020), including temperature, moisture, and vertical velocity, as an alternative. The ERA5 data are then linearly interpolated to the location of the coastal site in La Jolla. We have validated key meteorological variables including lower-tropospheric stability (LTS), the moisture contrast between the surface and 700 hPa (dq), and relative humidity at 700 hPa (RH_{700}), which are calculated from ERA5 against EPCAPE observations. Figure S3 in Supporting Information S1 illustrates bias metrics for these variables. We find that all correlation coefficients exceed 0.91, with small root mean squared errors (relative to the observed standard deviation), affirming the validity of using ERA5 as a reliable alternative to balloon radiosondes for obtaining vertical meteorological information. The large-scale vertical velocity and advective tendencies of temperature and moisture at the coastal site are derived from ERA5 through the constrained variational analysis approach (Xie et al., 2004; M. H. Zhang & Lin, 1997; M. H. Zhang et al., 2001).

2.3. Isolating Aerosol Effects on LWP From Meteorology

To explore the intricate relationships between LWP and its controlling factors, that is, MFs and aerosols, we employ a tree-based ML algorithm, namely the eXtreme Gradient Boosting Decision Tree (XGBoost, Chen & Guestrin, 2016). This algorithm achieves a scalable and accurate implementation of gradient boosting, outperforming traditional boosted tree models in speed. More importantly, XGBoost predictions are interpretable with a statistical approach. To build the ML model, eight MFs and one aerosol index (N_d) are chosen as predictors, based upon our previous work (Cao et al., 2024; H. Zhang et al., 2024a, 2024b). The selected MFs include LTS, dq, vertical velocity at 700 hPa (ω_{700}), RH_{700}, moisture advective tendency (q_{adv}) at 1,000 hPa, temperature advective tendency (T_{adv}) at 1,000 hPa, LHF, and horizontal wind speed at 10 m (U_{sfc}). These factors have been demonstrated to be the key cloud-controlling factors, each representing an explicit physical process. For example, LTS indicates the influence of lower-tropospheric static stability or cloud top inversion strength on cloud decks (Bretherton et al., 2013), and dq denotes the efficiency of entrainment of dry air from the free troposphere into cloud layers (van der Dussen et al., 2014), and more are detailed in Qu et al. (2015). Relative to H. Zhang et al. (2024b), this study introduces the moisture advection (q_{adv}) as a new predictor to account for the unique coastal dynamics influenced by the diurnal cycle of sea and land breezes, which leads to varying moisture sources. The predictors used in the ML model are summarized in Table 1. Note that the relationships explored here are based on concurrently observed LWP and influential factors. Aerosols may, however, exert a lagged effect on LWP, which is discussed in Text S2 in Supporting Information S1.

CCN observations began in late May 2023 and were unavailable in October 2023 (see Figure S2 in Supporting Information S1); consequently, we utilized roughly 7 months of hourly data at the coastal site for model training and testing, with an independent training/test split of approximately 70%/30%. The total sample sizes for training and testing are about 3,200 and 1,400 hr, respectively. For the training set, we standardize all input features or predictors by removing their means and scaling them to unit variance. Given the moderate size of our data set, we

19448007, 2025, 15, Downloaded from https://agupubs.onlinelibrary.wiley.com/doi/10.1029/2025GL115163 by University Of Houston, Wiley Online Library on [01/04/2026]. See the Terms and Conditions (https://onlinelibrary.wiley.com/terms-and-conditions) on Wiley Online Library for rules of use; OA articles are governed by the applicable Creative Commons License

Table 1
Summary of Nine Predictors Influencing Liquid Water Path in the Machine Learning Model

Factors	Description	Data sources
LTS	Lower-tropospheric stability (K)	ERA5
dq	Moisture contrast between 1,000 and 700 hPa (kg/kg)	ERA5
RH_{700}	Relative humidity at 700 hPa (%)	ERA5
ω_{700}	Large-scale vertical velocity at 700 hPa (hPa/hr)	VARANAL
q_{adv}	Horizontal moisture advection tendency (g/kg/hr) at 1,000 hPa	VARANAL
T_{adv}	Horizontal temperature advection tendency (K/hr) at 1,000 hPa	VARANAL
LHF	Latent heat flux (W/m^2)	EPCAPE
U_{sfc}	Near-surface winds at 10 m (m/s)	EPCAPE
N_d	Activated CCN number concentration (cm^{-3})	EPCAPE

opt not to use complex parameter tuning techniques, such as the Bayesian optimization (Snoek et al., 2012). Instead, through trial and error, we determine the values of two key parameters: max_depth and n_estimators, set at 5 and 15, respectively. Here, max_depth represents the maximum tree depth for base learners, while n_estimators denotes the number of gradient boosted trees. The model is trained 100 times to produce a 100-member ensemble by randomly separating the data set into training and test sets. The mean squared error (MSE) for the test set across most ensemble members stays within a 20% range of the training set's MSE, indicating that our model does not suffer from overfitting. On average, the ensemble members can explain 63.0% of the variation in hourly LWP, with a standard deviation of 1.7%.

To isolate the contribution of each influencing factor to predicted LWP, the SHAP (Lundberg & Lee, 2017; Lundberg et al., 2018) analysis is utilized to interpret the XGBoost predictions. This statistical approach is based on coalitional game theory, which calculates the contribution of a predictor as the difference between the XGBoost predictions (LWP in this study) in the presence and absence of this specific predictor for all possible predictor combinations. It explains a model's individual output as a sum of the contributions of each predictor plus the mean predicted value through an explanation model, which can be expressed as:

$$y = \bar{y} + \sum_i \phi_i, \tag{1}$$

where y is the final prediction for one case, $\bar{y}$ is the average prediction across all cases, and ϕ_i is the contribution of the ith predictor to the prediction for this case (called SHAP values). Therefore, for one specific prediction case, the LWP partially predicted by N_d can be denoted as

$$\mathrm{LWP}_{N_d} = \bar{y} + \phi_{N_d} \tag{2}$$

SHAP values are calculated using TreeSHAP, an efficient and exact algorithm for tree ensemble models, developed using the conditional expectation to estimate predictor's effects with no feature independence assumption required (Lundberg et al., 2018, 2020). The predictors with larger absolute SHAP values contribute more to LWP prediction than those with smaller values. We calculate SHAP values for all sample cases (including both training and test sets) within each ensemble member, and the ensemble-mean values are used for analysis in this study.

3. Results

3.1. Aerosol Effects on LWP

Figure 1 shows the importance of each influential factor to predicted LWP, quantified by the hourly (or case) mean absolute SHAP value of that factor within one ensemble member, then averaged across all members. To determine the relative perturbation of each factor compared to the base state of LWP in the ML model, the SHAP value is further normalized by the hourly mean LWP. It is evident that the contribution of aerosols to LWP outweighs that of any chosen MF, with dq and RH_{700} the most significant among them. These results, however,

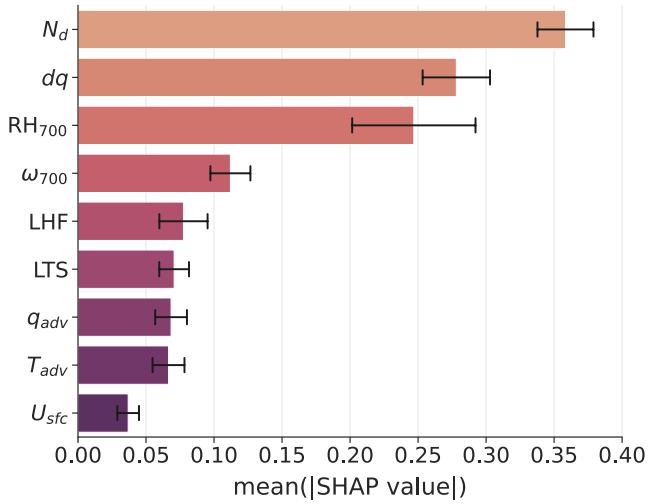


Figure 1. Bar plot of each predictor's absolute SHapley Additive exPlanations (SHAP) values averaged over cases and ensemble members by XGBoost, normalized by the mean liquid water path. Error bars indicate the standard deviation of the above SHAP values derived from 100 ensemble members.

may be subject to observational errors in CCN measurements and the ML model training process (e.g., the train-test split strategy). We have examined the LWP perturbation caused by N_d relative to the base state in the ML model, which is approximately 35%. This perturbation exceeds the typical uncertainty (10%–30%) of CCN measurement (Rissler et al., 2004), indicating that the aerosol signal in this study is robust. To minimize the influence of randomness, we train our ML model 100 times with random train-test splits. The error bars in Figure 1 indicate the standard deviation induced by these 100 ensemble members. The results show that the SHAP value of N_d is statistically distinguishable from those of dq and RH_{700}, confirming that the effect of aerosol on LWP is significantly larger than that of any MF. Our findings of the significant influence of aerosols on clouds, based on regional ground observations, are consistent with global satellite-based research. For example, using near-global satellite observations, Cao et al. (2024) found that N_d exhibits the most pronounced impact on low-level cloud cover, cloud albedo, and cloud radiative effects compared to MFs on daily scales, as revealed in a convolutional neural network using the permutation importance method.

We distinguish the effects of aerosols on clouds from meteorology through an explainable ML approach. Figure 2a shows the N_d-LWP relationship from the raw data, where aerosol and meteorological influences are mixed, obscuring the true interaction between aerosols and LWP. As expected, no clear pattern between LWP and N_d is found. With SHAP analysis, we can quantify the LWP contributed only by aerosol effects (LWP_{Nd}) via removing meteorological co-variabilities. The new relationship after employing SHAP analysis as displayed in Figure 2b uncovers a well-defined negative linear N_d-LWP relationship in log space, which may be explained by the N_d-induced entrainment drying effect on LWP, especially for the range of N_d between 250 and 800 cm^{-3}, which comprises 65.7% of all cases. This pattern aligns with the negative regime of the inverted-V relationship observed in previous studies (e.g., Hoffmann et al., 2024) but is shifted toward a more polluted scenario (or higher-N_d background). The positive regime is, however, not found in EPCAPE observations, likely because most cases are non-precipitating, resulting in no precipitation-suppression effect. These non-precipitating cases are indicated by the right area of the line of 15-μm cloud top effective droplet radius, commonly used to distinguish precipitating from non-precipitating clouds (e.g., Qiu et al., 2024). A comparison of Figure 2b with Figure 2a demonstrates the

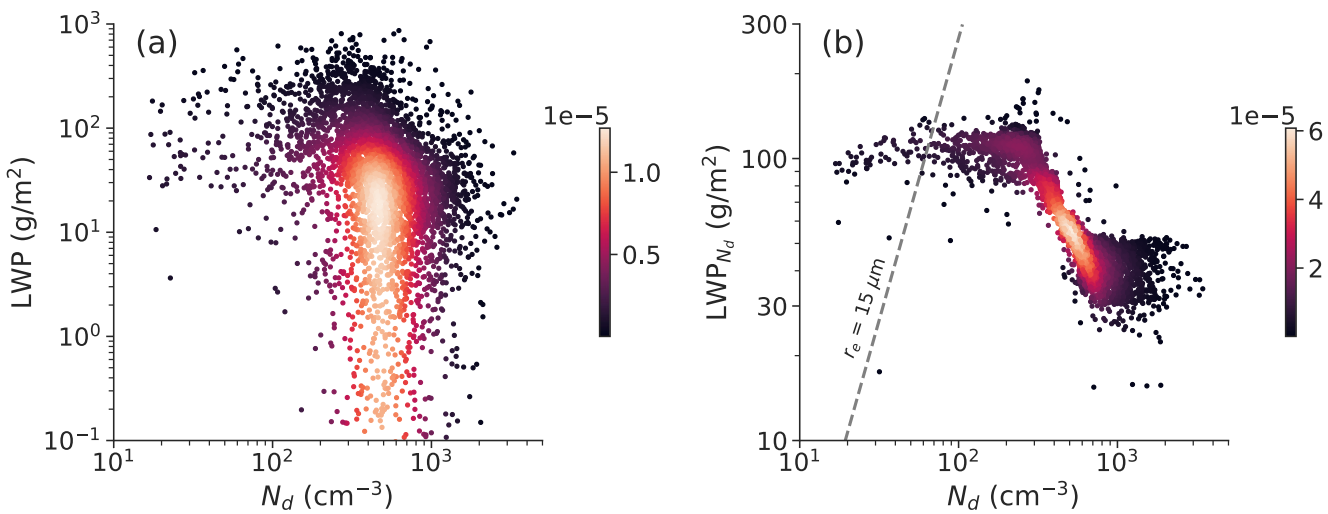


Figure 2. Relationship between hourly liquid water path (LWP) and N_d derived from Eastern Pacific Cloud Aerosol Precipitation Experiment observations. (a) The relationship when aerosol effects on LWP are co-influenced by large-scale meteorological factors like large-scale vertical velocity, surface winds, etc. (b) The relationship after removing meteorological effects using the SHapley Additive exPlanations analysis. The color bar indicates scatter density, and the dashed line in panel (b) represents the 15-μm cloud top effective droplet radius.

19448007, 2025, 15, Downloaded from https://agupubs.onlinelibrary.wiley.com/doi/10.1029/2025GL115163 by University Of Houston, Wiley Online Library on [01/04/2026]. See the Terms and Conditions (https://onlinelibrary.wiley.com/terms-and-conditions) on Wiley Online Library for rules of use; OA articles are governed by the applicable Creative Commons License

19448007, 2025, 15, Downloaded from https://agupubs.onlinelibrary.wiley.com/doi/10.1029/2025GL115163 by University Of Houston, Wiley Online Library on [01/04/2026]. See the Terms and Conditions (https://onlinelibrary.wiley.com/terms-and-conditions) on Wiley Online Library for rules of use; OA articles are governed by the applicable Creative Commons License

capability of this novel explainable ML approach to disentangle dynamical co-variability, offering valuable insights into the impact of aerosols on stratocumulus clouds and advancing our qualitative understanding of these complex interactions.

Similarly, we examine the meteorological controls on LWP after isolating aerosol effects, as shown in Figure S4 in Supporting Information S1. Compared to aerosol effects, meteorological controls are more complex, with some factors exhibiting linear relationships and others showing non-linear behavior. For linear relationships, LWP generally increases with RH_{700} and q_{adv} while decreasing with ω_{700}. The increases in LWP are caused by weakened entrainment drying due to offset cloud top radiative cooling (Myers & Norris, 2016; van der Dussen et al., 2015) and increased moisture sources, respectively. The decrease in LWP is induced by subsidence drying (van der Dussen et al., 2016). These findings agree with those of H. Zhang et al. (2023), in which these relationships are studied using LES modeling. These agreements demonstrate the effectiveness of explainable ML in helping understand physical controls on cloud properties. Those non-linear behaviors are detailed in Text S1 in Supporting Information S1.

3.2. Dependence of N_d-LWP Relationship

The aforementioned findings reveal a negative N_d-LWP relationship consistent with entrainment drying effects, which are inherently controlled by two factors, dq and LTS. dq governs the efficiency of the drying effects given the same level of turbulence (see Equation 1 in H. Zhang et al. (2023)), while LTS influences the strength of entrainment rate. In that regard, we next delve into the investigation of the dependence of the N_d-LWP relationship on those two factors. As shown in Figure 2b, the linear response of LWP_{Nd} to N_d in log space is most evident when N_d ranges between 250 and 800 cm^{-3}. This linear relationship disappears at lower N_d values due to insufficient precipitating cases and at higher N_d values due to saturated aerosol effects. Therefore, the slope of LWP_{Nd} versus N_d in the medium range of N_d (250–800 cm^{-3}) is calculated to represent the most significant linear response. Slight adjustments to these boundary values does not affect results. To explore how this response depends on dq and LTS, we sort data samples into 10 quantile bins based on dq or LTS values (Figures S6 and S7 in Supporting Information S1). Within each bin, the sensitivity of LWP to N_d is calculated using the above method, as summarized in Figures 3a and 3b.

Generally, the response of LWP to N_d exhibits a non-linear dependence on dq and LTS, as illustrated by the purple versus green boxes in Figures 3a and 3b. We assume this behavior arises from two competing effects: the direct influence of the MF on entrainment drying through changes in drying efficiency or entrainment strength, and its indirect influence via LWP modifications. As shown in Figure 3a, the sensitivity of LWP to N_d (measured by the magnitude of $d\ln LWP_{Nd}/d\ln N_d$) initially increases with dq and then decreases. The initial increase is linked to greater entrainment drying efficiency as dq rises. However, further increases in dq deplete LWP, and the resulting reduction in cloud top radiative cooling limits entrainment processes, leading to a weaker response of LWP to N_d (Figure 3c). A similar inverted-V relationship is observed for LTS (Figure 3b). At lower LTS, the sensitivity of LWP to N_d is enhanced because stronger LTS traps moisture in the PBL, increasing LWP and promoting cloud top entrainment. However, at higher LTS, the suppression of entrainment dominates, resulting in weaker sensitivities. These findings highlight the critical role of the interplay between MFs' direct and indirect effects on entrainment drying in shaping the N_d-LWP relationship. In addition to dq and LTS, the effects of RH_{700} and ω_{700} (two key contributors to LWP identified in Figure 1) on the LWP sensitivities are examined (Figure S8 in Supporting Information S1). Their impacts on LWP sensitivities are found to be relatively simpler or linear, as primarily driven by their influence on LWP.

We further analyze the diurnal cycle of LWP responses to N_d by sorting data into 24 local hourly bins and calculating the sensitivity for each bin (Figure 3d). The dashed lines indicate the sunrise and sunset times averaged across all sample days. The LWP sensitivities are notably weaker during the daytime (highlighted by the gray box in Figure 3d) than at night. The reduction is due to the weakened entrainment, resulting from the presence of solar radiation that offsets cloud top radiative cooling and a concurrent decrease in LWP. It is noted that the effects of solar radiation on LWP sensitivities are delayed by about 2 hours after sunrise and sunset. Also, the diurnal cycle of surface wind directions contributes to this pattern. During the daytime, sea breeze (Figure S9a in Supporting Information S1) induces anomalous downdrafts over the ocean (Figure S9b in Supporting Information S1), pushing downward the PBLH and reducing LWP, which further weakens the LWP response to N_d (Figure 3c).

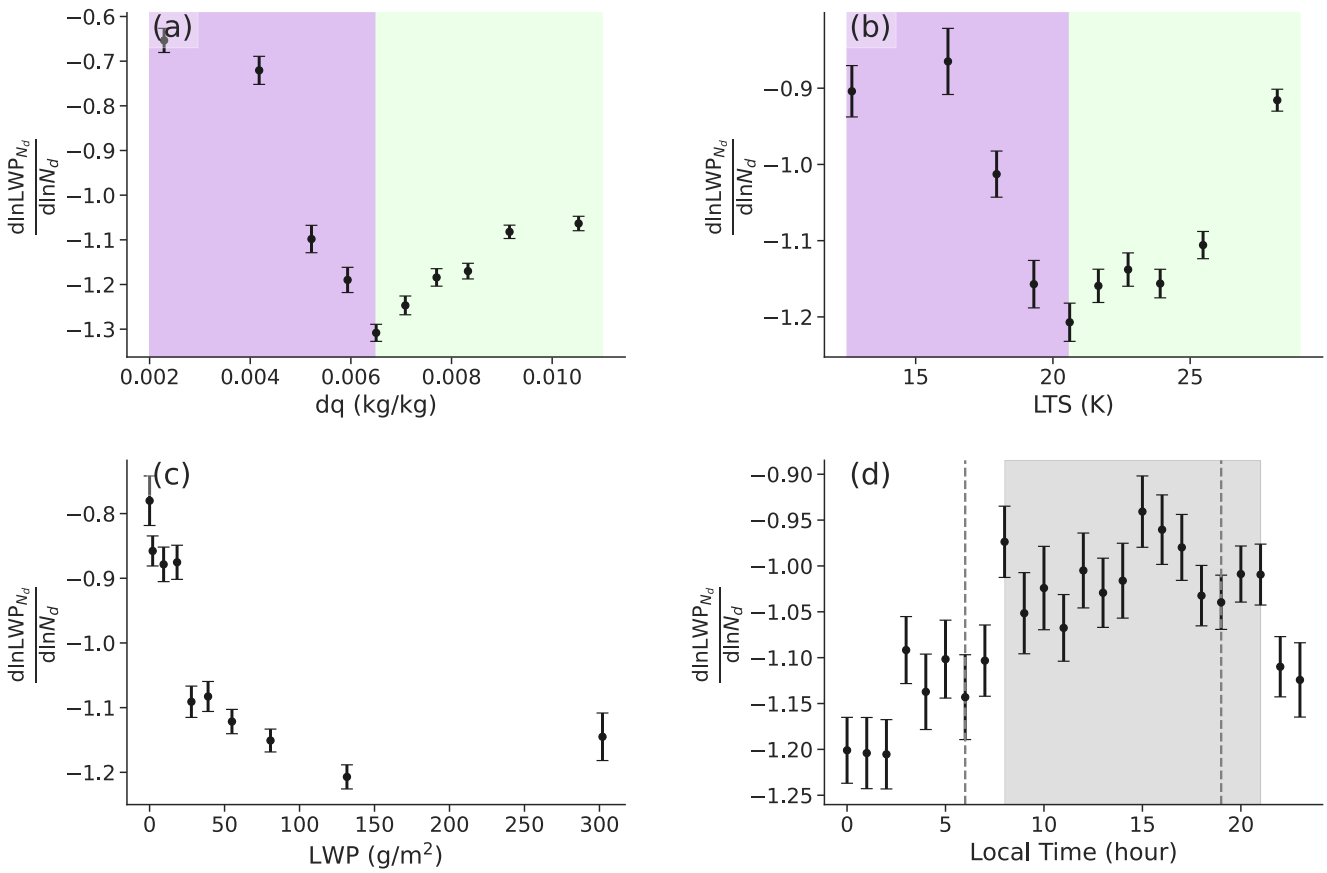


Figure 3. Dependence of the N_d-LWP_{Nd} relationship on various factors: (a) *dq*, (b) lower-tropospheric stability, (c) liquid water path, and (d) Local Time. In panels (a–c), the data are sorted into 10 quantile bins based on the respective factor, while in panel (d) they are binned into 24 hourly intervals. The sensitivity of LWP_{Nd} to N_d is calculated within each bin, with error bars representing the standard deviation of the sensitivity. The purple and green boxes in panels (a, b) mark the downward and upward trends, respectively. The dashed lines in panel (d) indicate the mean sunrise and sunset times, and the gray box marks the daytime period shifted 2 hours forward.

4. Discussion

In this study, the slope of the N_d-LWP relationship is obtained through SHAP analysis and corresponds to the partial derivative of LWP w.r.t. N_d, which isolates the individual effect of aerosols. In contrast, earlier studies (e.g., Hoffmann et al., 2024; Qiu et al., 2024) typically compute the full derivative, which inherently includes both aerosol and meteorology-mediated effects. The extent to which meteorological effects remain in those slopes depends on the sampling strategy. Overall, our slope (−1.1 in Figure 2b) is more negative than the full-derivative slopes that do not remove meteorological effects (e.g., around −0.4; see Figure 1a in Qiu et al. (2024)), while aligning more closely with those full-derivative slopes that reduce meteorological influences by classifying samples into different cloud regimes, for example, the slopes for non-precipitating cloud regimes range from −0.8 to −1.2 (see Figure 2a in Qiu et al. (2024)). A detailed discussion of slope definitions and their implications is provided in Text S3 in Supporting Information S1.

As for the underlying mechanism, the negative N_d-LWP relationship observed in our study is likely induced by the entrainment effect. However, previous studies have shown that synoptic-scale meteorological influences may also contribute, particularly through the airmass-history argument as discussed in the introduction. To test this possibility, we compute 24-hr backward trajectories using the HYSPLIT model and categorize each case based on airmass origin (oceanic or continental; Figure S11 in Supporting Information S1). Oceanic airmasses are found to be more humid and cleaner than continental ones (Figure S11c in Supporting Information S1 vs. Figure S11d in Supporting Information S1). If airmass history were the dominant factor, the N_d-LWP relationship would be weak or even disappear when the airmass origin is controlled. However, the negative correlation remains strong within

19448007, 2025, 15, Downloaded from https://agupubs.onlinelibrary.wiley.com/doi/10.1029/2025GL115163 by University Of Houston, Wiley Online Library on [01/04/2026]. See the Terms and Conditions (https://onlinelibrary.wiley.com/terms-and-conditions) on Wiley Online Library for rules of use; OA articles are governed by the applicable Creative Commons License

19448007, 2025, 15, Downloaded from https://agupubs.onlinelibrary.wiley.com/doi/10.1029/2025GL115163 by University Of Houston, Wiley Online Library on [01/04/2026]. See the Terms and Conditions (https://onlinelibrary.wiley.com/terms-and-conditions) on Wiley Online Library for rules of use; OA articles are governed by the applicable Creative Commons License

both oceanic and continental subsets (Figures S12a or S12b in Supporting Information S1), suggesting that airmass-history-induced covariability is not the primary driver.

Another way to assess the airmass-history hypothesis is to select an index that can reflect airmass history and examine its correlation with N_d and LWP. Prior studies (Goren et al., 2025; Mülmenstädt, Ackerman, et al., 2024; Possner et al., 2020) commonly use PBLH for this purpose. PBLH also proves to be a useful proxy in our study, as lower PBLH is significantly correlated with more negative moisture advection ($r = 0.4$), indicating continental airmass influence (Figure S11d in Supporting Information S1). To examine whether the N_d-LWP relationship is affected by meteorological covariability, we stratify the data into 4 quantile bins based on PBLH (Figure S13 in Supporting Information S1). In the middle PBLH range (Figures S13b and S13c in Supporting Information S1), where PBLH is uncorrelated with aerosols, the strong negative N_d-LWP relationship persists, suggesting it is not driven by meteorological variability. However, at the lowest and highest PBLH ranges, PBLH is correlated with both N_d and LWP, implying that meteorological covariance may exist under those conditions. However, considering the strong N_d-LWP correlation and the fact that PBLH explains only a small portion of the variance in N_d and LWP (Figure S13 in Supporting Information S1), such covariance is less likely to be the dominant factor.

Little covariance is observed within the middle PBLH range, likely because the main observation site, located along the coast, is subject to complex influences such as mesoscale circulation, the Catalina eddy, and sea breeze circulation. The role of subtropical anticyclonic subsidence in covariance, therefore, remains limited unless it remarkably influences airmass advections (indicated by the extreme low or high PBLH). While our results support a dominant causal role of aerosols, a more robust, process-level assessment using large-eddy simulations is needed to isolate aerosol effects under controlled meteorological conditions, which is beyond the scope of this study.

5. Summary

This study employs an interpretable ML framework (XGBoost-SHAP analysis) to disentangle aerosol influences on cloud water, using recent EPCAPE observations near the California coast. The ML model, XGBoost, is adopted to explore the relationship between cloud-controlling factors (N_d and key MFs) and LWP. SHAP analysis can help isolate the individual contribution of each factor to LWP prediction, revealing that aerosols predominantly explain the LWP variability compared to each MF in EPCAPE observations. This result is robust, with aerosol-induced perturbations to mean LWP exceeding the uncertainty of CCN measurements. Following aerosol effects, dq and RH_{700} are the top two meteorological contributors to LWP variability. By excluding meteorological influences, we find a significant negative linear relationship between LWP and N_d in log space, consistent with the negative regime (right branch) of the inverted-V relationship reported in previous studies, but in a more polluted environment. This negative response of LWP to N_d is more likely caused by the causal mechanism of entrainment drying, rather than by synoptic-scale meteorology induced covariance between N_d and LWP—particularly the airmass-history argument, as discussed in Section 4. The positive regime (left branch) of the inverted-V relationship is not observed in EPCAPE mainly because of the limited occurrence of precipitating cases during the observation period.

We also examine the dependence of LWP sensitivity to N_d on two MFs (dq and LTS), which essentially influence entrainment drying effects. The sensitivity exhibits a non-linear response to both factors, strengthening initially with increasing dq or LTS, then weakening beyond a threshold. For example, higher dq initially enhances entrainment drying efficiency, amplifying sensitivity, but excessive dq reduces LWP and suppresses radiative-cooling-driven entrainment, thereby diminishing sensitivity. This dynamic reflects a critical interplay between the direct effects of MFs on entrainment drying and their indirect influence via LWP adjustments. This study highlights the effectiveness of explainable ML in isolating aerosol effects on cloud properties and demonstrates its potential for broader application in other field campaigns. Furthermore, our findings uncover the complex meteorological controls on how aerosols impact clouds, offering valuable insights for improving warm-cloud microphysics parameterizations in climate models. The CCN counter data used in our study were reported to be affected by a leak in the CCN sample line (ARM User Facility, 2025). To confirm the robustness of our results, we repeated the analysis using CCN number concentrations predicted from the Aerosol Chemical Speciation Monitor (ACSM) and the Scanning Mobility Particle Sizer (SMPS) measurements, which are considered a more accurate reference. Our main conclusions remain unchanged. Further details are provided in Supporting Information S2.

Data Availability Statement

The EPCAPE observation data can be accessed at ARM user Facility (2024). The ERA5 reanalysis data are available at Hersbach et al. (2020). The 60-min ECMWF constrained variational analysis for EPCAPE can be accessed at Tao and Xie (2024). The R package "splitr" used to calculate backward trajectories is available at Lannone (2016).

Acknowledgments

Haipeng Zhang and Yunyan Zhang were mainly supported by LLNL-LDRD-24-ERD-019 project during the summer intern of HZ at LLNL. Yunyan Zhang also acknowledges support from the Department of Energy (DOE) Office of Science Atmospheric System Research (ASR) THREAD project (DOE-SCW1800). Zhanqing Li was supported by DOE ASR program (DESC0022919) and the National Science Foundation (AGS2126098). Youtong Zheng was supported by the DOE Early Career Grant (DE-SC0024185). Work at the Lawrence Livermore National Laboratory is performed under the auspices of the U.S. DOE by LLNL under Contract DE-AC52-07NA27344. We thank Michael Diamond and an anonymous reviewer for their constructive comments, which helped improve the clarity and rigor of our work. ChatGPT is used to assist with the editing of the manuscript.

References

Ackerman, A. S., Kirkpatrick, M. P., Stevens, D. E., & Toon, O. B. (2004). The impact of humidity above stratiform clouds on indirect aerosol climate forcing. *Nature*, *432*(7020), 1014–1017. https://doi.org/10.1038/nature03174

Albrecht, B. A. (1989). Aerosols, cloud microphysics, and fractional cloudiness. *Science*, *245*(4923), 1227–1230. https://doi.org/10.1126/science.245.4923.1227

ARM user Facility. (2024). ARM mobile facility (EPC) La Jolla, CA; AMF1 (main site for EPCAPE on Scripps Pier) (M1) [Dataset]. Retrieved from https://www.arm.gov/research/campaigns/amf2023epcape

Arola, A., Lipponen, A., Kolmonen, P., Virtanen, T. H., Bellouin, N., Grosvenor, D. P., et al. (2022). Aerosol effects on clouds are concealed by natural cloud heterogeneity and satellite retrieval errors. *Nature Communications*, *13*(1), 1–8. https://doi.org/10.1038/s41467-022-34948-5

Atmospheric Radiation Measurement (ARM) User Facility (2025). Leak affects cloud condensation nuclei data from 2 ARM campaigns. Data Announcements, 2 June. Retrieved from https://www.arm.gov/news/data/post/104948

Bellouin, N., Quaas, J., Gryspeerdt, E., Kinne, S., Stier, P., Watson-Parris, D., et al. (2020). Bounding global aerosol radiative forcing of climate change. *Reviews of Geophysics*, *58*(1), 1–45. https://doi.org/10.1029/2019RG000660

Bretherton, C., Blossey, P. N., & Jones, C. R. (2013). Mechanisms of marine low cloud sensitivity to idealized climate perturbations: A single-LES exploration extending the CGILS cases. *Journal of Advances in Modeling Earth Systems*, *5*(2), 316–337. https://doi.org/10.1002/jame.20019

Bretherton, C., Blossey, P. N., & Uchida, J. (2007). Cloud droplet sedimentation, entrainment efficiency, and subtropical stratocumulus albedo. *Geophysical Research Letters*, *34*(3), L03813. https://doi.org/10.1029/2006GL027648

Cao, Y., Zhu, Y., Wang, M., Rosenfeld, D., Zhou, C., Liu, J., et al. (2024). Improving prediction of marine low clouds using cloud droplet number concentration in a convolutional neural network. *Journal of Geophysical Research: Machine Learning and Computation*, *1*(4), 1–16. https://doi.org/10.1029/2024JH000355

Chen, T., & Guestrin, C. (2016). XGBoost: A scalable tree boosting system. In *Proceedings of the ACM SIGKDD international conference on knowledge discovery and data mining* (Vol. 13, pp. 785–794). Association for Computing Machinery. https://doi.org/10.1145/2939672.2939785

Chun, J. Y., Wood, R., Blossey, P., & Doherty, S. J. (2023). Microphysical, macrophysical, and radiative responses of subtropical marine clouds to aerosol injections. *Atmospheric Chemistry and Physics*, *23*(2), 1345–1368. https://doi.org/10.5194/acp-23-1345-2023

Cook, D. R., & Sullivan, R. C. (2020). *Eddy correlation flux measurement system (ECOR) instrument handbook*. DOE/SC-ARM-TR-052. Retrieved from http://scholar.google.com/scholar?hl=en&btnG=Search&q=intitle:Eddy+Correlation+Flux+Measurement+System+Handbook#0

Fons, E., Runge, J., Neubauer, D., & Lohmann, U. (2023). Stratocumulus adjustments to aerosol perturbations disentangled with a causal approach. *Npj Climate and Atmospheric Science*, *6*(1), 1–10. https://doi.org/10.1038/s41612-023-00452-w

George, R. C., & Wood, R. (2010). Subseasonal variability of low cloud radiative properties over the southeast Pacific Ocean. *Atmospheric Chemistry and Physics*, *10*(8), 4047–4063. https://doi.org/10.5194/acp-10-4047-2010

Goren, T., Choudhury, G., Kretzschmar, J., & McCoy, I. (2025). Co-variability drives the inverted-V sensitivity between liquid water path and droplet concentrations. *Atmospheric Chemistry and Physics*, *25*(6), 3413–3423. https://doi.org/10.5194/acp-25-3413-2025

Gryspeerdt, E., Goren, T., Sourdeval, O., Quaas, J., Mülmenstädt, J., Dipu, S., et al. (2019). Constraining the aerosol influence on cloud liquid water path. *Atmospheric Chemistry and Physics*, *19*(8), 5331–5347. https://doi.org/10.5194/acp-19-5331-2019

Hahn, C. J., & Warren, S. G. (2007). *A gridded climatology of clouds over land (1971–96) and ocean (1954–97) from surface observations worldwide*. Oak Eidge, TN. https://doi.org/10.3334/CDIAC/cli.ndp026e

Heffter, J. (1980). Transport layer depth calculations. In *Second joint conference on applications of air pollution meteorology*. New Orleans, Louisiana.

Hersbach, H., Bell, B., Berrisford, P., Biavati, G., Horányi, A., Muñoz-Sabater, J., et al. (2020). The ERA5 global reanalysis [Dataset]. *Copernicus Climate Change Service (C3S) Climate Data Store (CDS)*. https://doi.org/10.24381/cds.bd0915c6

Hoffmann, F., Glassmeier, F., & Feingold, G. (2024). The impact of aerosol on cloud water: A heuristic perspective. *Atmospheric Chemistry and Physics*, *24*(23), 13403–13412. https://doi.org/10.5194/acp-24-13403-2024

Hoffmann, F., Glassmeier, F., Yamaguchi, T., & Feingold, G. (2020). Liquid water path steady states in stratocumulus: Insights from process-level emulation and mixed-layer theory. *Journal of the Atmospheric Sciences*, *77*(6), 2203–2215. https://doi.org/10.1175/JAS-D-19-0241.1

Holdridge, D., & Holdridge, G. (2020). *Balloon-borne sounding system (SONDE) instrument handbook*. ARM-TR-029. DOE Office of Science, Office of Biological and Environmental Research. Retrieved from https://www.science.org

Jia, Y., Andersen, H., & Cermak, J. (2024). Analysis of cloud fraction adjustment to aerosols and its dependence on meteorological controls using explainable machine learning. *Atmospheric Chemistry and Physics*, *24*(22), 13025–13045. https://doi.org/10.5194/acp-24-13025-2024

Kyrouac, J., & Tuftedal, M. (2024). *Surface meteorological system (MET) instrument handbook*. DOE/SC-ARM-TR-086. Retrieved from https://www.arm.gov/publications/tech_reports/handbooks/met_handbook.pdf

Lannone, R. (2016). splitr v0.4 [Software]. *GitHub repository*. Retrieved from https://github.com/rich-iannone/splitr

Liu, J., Zhu, Y., Yuan, T., Wang, M., Rosenfeld, D., & Cao, Y. (2024). Cloud susceptibility to aerosols: Comparing cloud - Appearance versus cloud - controlling factors regimes. *Journal of Geophysical Research: Atmospheres*, *129*(14), 1–18. https://doi.org/10.1029/2024JD041216

Lundberg, S. M., & Lee, S.-I. (2017). A unified approach to interpreting model predictions. *Advances in Neural Information Processing Systems*, *30*, 4766–4775. Retrieved from http://arxiv.org/abs/1705.07874

Lundberg, S. M., Erion, G., Chen, H., DeGrave, A., Prutkin, J. M., Nair, B., et al. (2020). From local explanations to global understanding with explainable AI for trees. *Nature Machine Intelligence*, *2*(1), 56–67. https://doi.org/10.1038/s42256-019-0138-9

Lundberg, S. M., Erion, G. G., & Lee, S.-I. (2018). Consistent individualized feature attribution for tree ensembles. Retrieved from http://arxiv.org/abs/1802.03888

19448007, 2025, 15, Downloaded from https://agupubs.onlinelibrary.wiley.com/doi/10.1029/2025GL115163 by University Of Houston, Wiley Online Library on [01/04/2026]. See the Terms and Conditions (https://onlinelibrary.wiley.com/terms-and-conditions) on Wiley Online Library for rules of use; OA articles are governed by the applicable Creative Commons License

Mülmenstädt, J., Ackerman, A. S., Fridlind, A. M., Huang, M., Ma, P., Mahfouz, N., et al. (2024). Can general circulation models (GCMs) represent cloud liquid water path adjustments to aerosol–cloud interactions? *Atmospheric Chemistry and Physics*, *24*(23), 13633–13652. https://doi.org/10.5194/acp-24-13633-2024

Mülmenstädt, J., Gryspeerdt, E., Dipu, S., Quaas, J., Ackerman, A. S., Fridlind, A. M., et al. (2024). General circulation models simulate negative liquid water path-droplet number correlations, but anthropogenic aerosols still increase simulated liquid water path. *Atmospheric Chemistry and Physics*, *24*(12), 7331–7345. https://doi.org/10.5194/acp-24-7331-2024

Myers, T. A., & Norris, J. R. (2016). Reducing the uncertainty in subtropical cloud feedback. *Geophysical Research Letters*, *43*(5), 2144–2148. https://doi.org/10.1002/2015GL067416

Possner, A., Eastman, R., Bender, F., & Glassmeier, F. (2020). Deconvolution of boundary layer depth and aerosol constraints on cloud water path in subtropical stratocumulus decks. *Atmospheric Chemistry and Physics*, *20*(6), 3609–3621. https://doi.org/10.5194/acp-20-3609-2020

Qiu, S., Zheng, X., Painemal, D., Terai, C. R., & Zhou, X. (2024). Daytime variation in the aerosol indirect effect for warm marine boundary layer clouds in the eastern North Atlantic. *Atmospheric Chemistry and Physics*, *24*(5), 2913–2935. https://doi.org/10.5194/acp-24-2913-2024

Qu, X., Hall, A., Klein, S. A., & Deangelis, A. M. (2015). Positive tropical marine low-cloud cover feedback inferred from cloud-controlling factors. *Geophysical Research Letters*, *42*(18), 7767–7775. https://doi.org/10.1002/2015GL065627

Rissler, J., Swietlicki, E., Zhou, J., Roberts, G., Andreae, M. O., Gatti, L. V., & Artaxo, P. (2004). Physical properties of the sub-micrometer aerosol over the Amazon rain forest during the wet-to-dry season transition - Comparison of modeled and measured CCN concentrations. *Atmospheric Chemistry and Physics*, *4*(8), 2119–2143. https://doi.org/10.5194/acp-4-2119-2004

Russell, L., Lubin, D., Silber, I., Eloranta, E., Muelmenstaedt, J., Burrows, S., et al. (2021). Eastern Pacific Cloud Aerosol Precipitation Experiment (EPCAPE) science plan. Doe/Sc-Arm-21-009.

Silva, S. J., Keller, C. A., & Hardin, J. (2022). Using an explainable machine learning approach to characterize Earth system model errors: Application of SHAP analysis to modeling lightning flash occurrence. *Journal of Advances in Modeling Earth Systems*, *14*(4). https://doi.org/10.1029/2021MS002881

Snoek, J., Larochelle, H., Adams, R. P., & Jeffery, C. (2012). Practical Bayesian optimization of machine learning algorithms. *Religion and the Arts*, *17*(1–2), 57–73. https://doi.org/10.48550/ARXIV.1206.2944

Tao, C., & Xie, S. (2024). Constrained variational analysis (60VARANAECMWF) [Dataset]. *Atmospheric Radiation Measurement (ARM) User Facility*. https://doi.org/10.5439/1860369

Turner, D. D., Clough, S. A., Liljegren, J. C., Clothiaux, E. E., Cady-Pereira, K. E., & Gaustad, K. L. (2007). Retrieving liquid water path and precipitable water vapor from the atmospheric radiation measurement (ARM) microwave radiometers. *IEEE Transactions on Geoscience and Remote Sensing*, *45*, 3680–3689. https://doi.org/10.1109/TGRS.2007.903703

Twomey, S. (1977). The influence of pollution on the shortwave albedo of clouds. *Journal of the Atmospheric Sciences*, *34*(7), 1149–1152. https://doi.org/10.1175/1520-0469(1977)034<1149:TIOPOT>2.0.CO;2

Uin, J., & Enekwizu, O. (2024). *Cloud condensation nuclei particle counter instrument handbook*. DOE/SC-ARM-TR-168. Retrieved from https://www.arm.gov/publications/tech_reports/handbooks/ccn_handbook.pdf

van der Dussen, J. J., De Roode, S. R., Gesso, S. D., & Siebesma, A. P. (2015). An LES model study of the influence of the free tropospheric thermodynamic conditions on the stratocumulus response to a climate perturbation. *Journal of Advances in Modeling Earth Systems*, *7*(2), 670–691. https://doi.org/10.1002/2014MS000380

van der Dussen, J. J., De Roode, S. R., & Siebesma, A. P. (2014). Factors controlling rapid stratocumulus cloud thinning. *Journal of the Atmospheric Sciences*, *71*(2), 655–664. https://doi.org/10.1175/JAS-D-13-0114.1

van der Dussen, J. J., De Roode, S. R., & Siebesma, A. P. (2016). How large-scale subsidence affects stratocumulus transitions. *Atmospheric Chemistry and Physics*, *16*(2), 691–701. https://doi.org/10.5194/acp-16-691-2016

Wang, H., Rasch, P. J., & Feingold, G. (2011). Manipulating marine stratocumulus cloud amount and albedo: A process-modelling study of aerosol-cloud-precipitation interactions in response to injection of cloud condensation nuclei. *Atmospheric Chemistry and Physics*, *11*(9), 4237–4249. https://doi.org/10.5194/acp-11-4237-2011

Wang, S., Wang, Q., & Feingold, G. (2003). Turbulence, condensation, and liquid water transport in numerically simulated nonprecipitating stratocumulus clouds. *Journal of the Atmospheric Sciences*, *60*(2), 262–278. https://doi.org/10.1175/1520-0469(2003)060<0262:TCALWT>2.0.CO;2

Wang, Z., Mora Ramirez, M., Dadashazar, H., MacDonald, A. B., Crosbie, E., Bates, K. H., et al. (2016). Contrasting cloud composition between coupled and decoupled marine boundary layer clouds. *Journal of Geophysical Research: Atmospheres*, *121*(19), 238. https://doi.org/10.1002/2016JD025695

Warren, S. G., Hahn, C. J., London, J., Chervin, R. M., & Jenne, R. L. (1986). *Global distribution of total cloud and cloud type amounts over land*. National Center for Atmospheric Research. https://doi.org/10.5065/D6GH9FXB

Warren, S. G., Hahn, C. J., London, J., Chervin, R. M., & Jenne, R. L. (1988). Global distribution of total cloud cover and cloud type amounts over the ocean. Retrieved from https://www.osti.gov/servlets/purl/5415329

Xie, S., Cederwall, R. T., & Zhang, M. (2004). Developing long-term single-column model/cloud system-resolving model forcing data using numerical weather prediction products constrained by surface and top of the atmosphere observations. *Journal of Geophysical Research*, *109*(1), D01104. https://doi.org/10.1029/2003jd004045

Xue, H., & Feingold, G. (2006). Large-eddy simulations of trade wind cumuli: Investigation of aerosol indirect effects. *Journal of the Atmospheric Sciences*, *63*(6), 1605–1622. https://doi.org/10.1175/JAS3706.1

Zhang, H., Zheng, Y., Lee, S. S., & Li, Z. (2023). Surface-atmosphere decoupling prolongs cloud lifetime under warm advection due to reduced entrainment drying. *Geophysical Research Letters*, *50*(10), e2022GL101663. https://doi.org/10.1029/2022GL101663

Zhang, H., Zheng, Y., & Li, Z. (2024a). Evaluation of stratocumulus evolution under contrasting temperature advections in CESM2 through a Lagrangian framework. *Geophysical Research Letters*, *51*(4), e2023GL106856. https://doi.org/10.1029/2023GL106856

Zhang, H., Zheng, Y., & Li, Z. (2024b). Improving low-cloud fraction prediction through machine learning. *Geophysical Research Letters*, *51*(15), e2024GL109735. https://doi.org/10.1029/2024GL109735

Zhang, M. H., & Lin, J. L. (1997). Constrained variational analysis of sounding data based on column-integrated budgets of mass, heat, moisture, and momentum: Approach and application to ARM measurements. *Journal of the Atmospheric Sciences*, *54*(11), 1503–1524. https://doi.org/10.1175/1520-0469(1997)054<1503:CVAOSD>2.0.CO;2

Zhang, M. H., Lin, J. L., Cederwall, R. T., Yio, J. J., & Xie, S. C. (2001). Objective analysis of ARM IOP data: Method and sensitivity. *Monthly Weather Review*, *129*(2), 309–311. https://doi.org/10.1175/1520-0493(2001)129<0295:oaoaid>2.0.co;2

19448007, 2025, 15, Downloaded from https://agupubs.onlinelibrary.wiley.com/doi/10.1029/2025GL115163 by University Of Houston, Wiley Online Library on [01/04/2026]. See the Terms and Conditions (https://onlinelibrary.wiley.com/terms-and-conditions) on Wiley Online Library for rules of use; OA articles are governed by the applicable Creative Commons License

References From the Supporting Information

Eastman, R., Terai, C. R., Grosvenor, D. P., & Wood, R. (2021). Evaluating the Lagrangian evolution of subtropical low clouds in GCMs using observations: Mean evolution, time scales, and responses to predictors. *Journal of the Atmospheric Sciences*, *78*(2), 553–572. https://doi.org/10.1175/JAS-D-20-0178.1

Glassmeier, F., Hoffmann, F., Johnson, J. S., Yamaguchi, T., Carslaw, K. S., & Feingold, G. (2021). Aerosol-cloud-climate cooling overestimated by ship-track data. *Science*, *371*(6528), 485–489. https://doi.org/10.1126/science.abd3980

Gryspeerdt, E., Goren, T., & Smith, T. W. P. (2021). Observing the timescales of aerosol-cloud interactions in snapshot satellite images. *Atmospheric Chemistry and Physics*, *21*(8), 6093–6109. https://doi.org/10.5194/acp-21-6093-2021

Erratum

The originally published version of this article contained errors. The following has been added to the end of Section 5: "The CCN counter data used in our study were reported to be affected by a leak in the CCN sample line (ARM User Facility, 2025). To confirm the robustness of our results, we repeated the analysis using CCN number concentrations predicted from the Aerosol Chemical Speciation Monitor (ACSM) and the Scanning Mobility Particle Sizer (SMPS) measurements, which are considered a more accurate reference. Our main conclusions remain unchanged. Further details are provided in Supporting Information S2." The following reference has been added to the References: Atmospheric Radiation Measurement (ARM) User Facility (2025). Leak affects cloud condensation nuclei data from 2 ARM campaigns. Data Announcements, 2 June. Retrieved from https://www.arm.gov/news/data/post/104948. In addition, Supporting Information S2 has been newly added. This may be considered the authoritative version of record.

19448007, 2025, 15, Downloaded from https://agupubs.onlinelibrary.wiley.com/doi/10.1029/2025GL115163 by University Of Houston, Wiley Online Library on [01/04/2026]. See the Terms and Conditions (https://onlinelibrary.wiley.com/terms-and-conditions) on Wiley Online Library for rules of use; OA articles are governed by the applicable Creative Commons License